Published in final edited form as:
J Phys Chem C Nanomater Interfaces. 2012 August 16; 116(32): 16918–168924. doi:10.1021/jp3059382.

A Tetrapyrrole Macrocycle Displaying a Multielectron Redox Chemistry and Tunable Absorbance Profile

Allen J. Pistner, **Glenn P. A. Yap**, and **Joel Rosenthal***
Department of Chemistry and Biochemistry, University of Delaware, Newark, DE 19716.

Abstract

Porphyrins are attractive chromophores for incorporation into light harvesting devices. Some of the most efficient porphyrin derivatives in this regard are synthetically complex platforms with specially tailored electronic properties. This work details the unique geometric and electronic structure of the phlorin framework. X-ray crystallography and NMR spectroscopy demonstrate that unlike typical tetrapyrrole macrocycles, the phlorin is not aromatic. These unusual electronics are manifest in distinct photophysical and redox properties, as the phlorin displays a rich multielectron redox chemistry. The phlorin also displays an intriguing supramolecular chemistry and can reversibly bind up to two equivalents of fluoride in cooperative fashion. Accordingly, this synthetically accessible sensitizer displays a rich multielectron redox chemistry, excellent spectral coverage and an intriguing anion binding chemistry that distinguishes this system from more commonly studied porphyrinoids.

Keywords

Phlorin; Porphyrin; Corrole; DSC; Solar Energy

INTRODUCTION

Nature can proficiently harvest sunlight using various chlorophylls, which are natural porphyrin based chromophores.[1] Accordingly, porphyrin derivatives have been featured prominently in studies dealing with the fabrication and photophysical interrogation of TiO_2 based Dye-Sensitized Solar Cells (DSCs),[2,3] in which the tetrapyrrole macrocycle serves as the light absorber and sensitizer.[4] Although much effort has been directed toward the incorporation of porphyrin sensitizers into DSCs, conversion efficiencies exhibited for this class of dye have historically fallen below that obtained using more expensive ruthenium based chromophores.[5] Indeed, it is only within the last five years that porphyrin based DSCs have achieved efficiencies above 7%.[6] Recent work, however, has demonstrated that attenuation of the porphyrin electronic properties is manifest in improved light harvesting ability. In particular, incorporation of redox active substituents onto the macrocycle periphery[7,8] and extension of the π-electron system[9–12] yield porphyrin sensitizers that display enhanced electron donation and improved light absorption properties at the low energy end of the visible region.[13] Highly derivatized porphyrin constructs of this type

*Corresponding Author rosenthal@mail.chem.udel.edu.

Author Contributions The manuscript was written through contributions of all authors. All authors have given approval to the final version of the manuscript.

Supporting Information Experimental details, spectroscopic and crystallographic data. This material is available free of charge via the Internet at http://pubs.acs.org. Crystallographic data are also available from the Cambridge Crystallographic Data Centre (CCDC 878742).

possess a multielectron redox chemistry and have been incorporated into DSCs that exhibit record power conversion efficiencies that are in excess of 12%.[14]

A significant reason why the privileged porphyrin constructs described above have given rise to high-efficiency DSCs is the fact that these elaborate dyes display strongly absorbing bands at long wavelengths ($\lambda > 600$ nm), while simpler porphyrin derivatives that lack ancillary donor groups and conjugated bridges do not effectively collect photons at the low energy end of the visible spectrum. Elaborate porphyrin syntheses are commensurate with these improved photophysical properties and add significantly to the complexity and cost associated with use of these dyes. As such, despite the advances in DSC efficiency that these highly derivatized porphyrins have enabled, the widespread use of DSCs would benefit from the development of a more synthetically accessible porphyrinoid platform that supports a multielectron redox chemistry and exhibits an absorbance profile that is well matched to the solar power spectrum (SPS) at long wavelengths.

In designing a porphyrinoid that can engender a multielectron reactivity, we considered a tetrapyrrole macrocycle that is related to the porphyrin. Porphyrinoids that contain tetrahedral *meso*-carbons have been constructed[15–17] and recent work has demonstrated that compounds of this type can exhibit a multielectron reactivity.[18] In particular, porphyrinogens containing dimethyl substituents at the *meso*-positions (Scheme 1) support multielectron oxidations,[19,20] which is a targeted property for a DSC sensitizer. However, the lack of conjugation between the pyrrole units of this macrocycle precludes the viability of absorption bands in the visible region and as a result, octamethylporphyrinogen is a white crystalline solid. Accordingly, we have sought to investigate porphyrinoid hybrids, which marry the photophysical properties of porphyrins with the rich redox chemistry of porphyrinogens (Scheme 1) by installing a single sp^3-hybridized carbon at one of the porphyrinoid *meso*-positions. Macrocycles of this type have been termed phlorins and we expected that this platform would display strong absorbances in the UV-vis region, given that conjugation across all four pyrrole units is maintained for this system. Herein we detail the basic photophysical and redox properties of the phlorin construct and show this platform possesses a multielectron photochemistry with an absorption profiled that can be easily tuned by via supramolecular binding of fluoride anions. These properties are discussed in terms of those inherent to more commonly studied polypyrrole macrocycles including porphyrins, calixpyrroles and corroles.

EXPERIMENTAL

General experimental methods and synthetic protocols are provided in the Supporting Information.

UV-vis Absorption Experiments

UV/visible absorbance spectra were acquired on a StellarNet CCD array UV-vis spectrometer using screw cap quartz cuvettes (7q) of 1 cm pathlength from Starna. All absorbance spectra were recorded at room temperature. All samples for spectroscopic analysis were prepared in dry THF within a N_2 filled glovebox. TBAF titrations experiments were conducted by placing 2.5 mL of a 10 μM solutions of 3H(Phl^F) in THF into a screw cap quartz cuvette. Following the recording of an initial UV-vis absorbance spectrum, 10 – 50 μL aliquots of a 0.1 mM solution of TBAF and 3H(Phl^F) (10 μM) in THF were added to the cuvette and changes in the UV-vis profile were monitored. Since the aliquots were all 10 μM in 3H(Phl^F), the concentration of phlorin did not change over the course of the experiment, which significantly simplifies analysis of the titration data. Job analysis for fluoride binding to 3H(Phl^F) was carried out using solutions containing 10 μM of total analyte (TBAF + 3H(Phl^F)) in THF. The ratio of phlorin to fluoride was systematically

varied by combining the appropriately sized aliquots of 10 mM stock solutions of TBAF and 3H(Phl^F) in THF.

Steady-State Fluorescence

Spectra were recorded on an automated Photon Technology International (PTI) QuantaMaster 40 fluorometer equipped with a 75-W Xenon arc lamp, a LPS-220B lamp power supply and a Hamamatsu R2658 photomultiplier tube. Samples for fluorescence analysis were prepared in an analogous method to that described above for the preparation of samples for UV-vis spectroscopy. Samples of 3H(Phl^F) were excited at λ = 630 nm and emission was monitored from 650–900 nm with a step size of 0.5 nm and integration time of 0.25 seconds. Reported spectra are the average of at least five individual acquisitions.

Electrochemical Measurements

Cyclic voltammetry was performed in a N_2 filled glove box using a CHI-760D bipoteniostat and a standard three-electrode assembly. CV scans were recorded for quiescent solutions using a glassy carbon working disk electrode (3.0 mm diameter), a platinum wire auxiliary electrode and a silver wire quasi-reference electrode. CV experiments were performed in CH_2Cl_2 with 0.1 M Tetrabutylammonium hexafluorophosphate ($TBAPF_6$) as the supporting electrolyte. Concentrations of phlorin analytes were 1 mM and a scan rate of 50 mV/s and sensitivity of 10 μA/V were maintained during data acquisition. All potentials are referenced relative to Ag/AgCl using a decamethylferrocenium– decamethylferrocene internal standard of 31 mV vs. Ag/AgCl.[21]

Spectroelectrochemical studies were performed in an optically transparent 1 mm thin-layer cell containing a ~0.1 mM solution of 3H(Phl^F) in THF containing 0.1 M tetrabutylammonium perchlorate (TBAP). The cell was equipped with a platinum mesh working electrode, a silver wire quasi-reference electrode, and a platinum wire auxiliary electrode. Oxidations were first carried out at 800 mV versus the reference electrode and absorbance spectra were recorded at one minute intervals. The potential was then increased to 1.1 V versus the reference electrode and absorbance spectra were again recorded at one minute intervals.

^{1}H and ^{19}F NMR Spectroscopy

NMR spectra were recorded at 25 °C on a Bruker 400 MHz spectrometer. Proton spectra are referenced to the residual proton resonance of the deuterated solvent ($CDCl_3$ = δ 7.26) and fluorine spectra are referenced to the fluorine resonances of an internal standard of trifluoroacetic acid (CF_3CO_2H = δ –76.55). All chemical shifts are reported using the standard δ notation in parts-per-million; positive chemical shifts are to higher frequency from the given reference.

X-ray Structural Solution and Refinement

Crystals of 3H(Phl^F) were mounted using viscous oil onto a plastic mesh and cooled to the data collection temperature. Data were collected on a Bruker-AXS APEX 2 DUO CCD diffractometer with Cu-Kα radiation (λ=1.54178 Å) collimated and monochromated using Goebel mirrors. Unit cell parameters were obtained from 60 data frames, 0.5° ω, from three different sections of the Ewald sphere. The systematic absences in the diffraction data are consistent with $P2_1$ and $P2_1/m$ but the observed occupancy and the absence of a molecular mirror is consistent with the noncentrosymmetric $P2_1$ which yielded chemically reasonable and computationally stable results of refinement. The absolute structure parameter was refined to 0.06(2) indicating the true hand of the data has been determined and an inspection of the packing diagram suggests no overlooked symmetry. The data set was treated with

numerical absorption corrections based on indexed crystal faces and dimensions (Apex2 software suite, Madison, WI, 2005). The structure was solved using direct methods and refined with full-matrix, least-squares procedures on F^2.[22] A disordered, cocrystallized molecule of chloroform solvent was located in the asymmetric unit with a refined site occupancy ratio of 56/44. The 1,1 and 1,2 interatomic distances were restrained to be equal in the disordered solvent molecule, treated with rigid bond restraints and with the carbon atom disordered contributions constrained to have equal anisotropic parameters. All non-hydrogen atoms were refined with anisotropic displacement parameters. All hydrogen atoms were treated as idealized contributions. Atomic scattering factors are contained in the SHELXTL 6.12 program library. The CIFs are available from the Cambridge Crystallographic Data Centre under the depositary numbers CCDC 878742.

RESULTS AND DISCUSSION

Initial reports of phlorin syntheses involved the addition of alkyl lithium reagents to porphyrins to generate a trianionic macrocycle in which a single *meso*-carbon is tetrahedral.[23] The synthesis and isolation of this porphyrinoid has also been carried out using typical acid catalysis,[24] and Geier and coworkers have described a pioneering general phlorin synthesis.[25] However, the electrochemical, photophysical and other basic properties of the phlorin have escaped characterization. We began our studies by preparing a 5,5-dimethyl phlorin architecture containing ancillary pentafluorophenyl groups (3H(Phl^F)),[25] the solid-state structure of which is shown in Figure 1. Accordingly, 3H(Phl^F) represents the first structurally characterized free base phlorin with a single sp^3-hybridized *meso*-carbon. Crystallographic parameters for this structure are provided in Table 1 and structural metrics are tabulated in the Supporting Information. Evaluation of the solid-state structure of 3H(Phl^F) indicates that unlike typical porphyrins, the phlorin macrocycle is not aromatic. This fact is demonstrated by the severe puckering of the reduced half of the macrocycle, which contains the 5,5-dimethyl substituent above the plane approximated by the other dipyrrole unit of the molecule by roughly 0.6 Å. The lack of aromaticity is also evident from ^{1}H NMR spectroscopy. The pyrrole N–H protons of typical tetraarylporphyrins are strongly shielded and display ^{1}H NMR resonances far upfield (–3.7 ppm for 2H(TPP))[26] due to magnetically induced diatropic ring currents[27–29] that flow around the macrocycle.[30] By contrast, the N–H protons of 3H(Phl^F) are far more deshielded, as characterized by a broad ^{1}H NMR resonance at 5.15 ppm in $CDCl_3$ (Figure S2). The aromatic fluorinated porphyrin homologue 2H(TpFPP) displays N–H resonances at –2.9 ppm in $CDCl_3$.

The unusual structure of 3H(Phl^F) is manifest in electronic properties that are disparate to those of typical porphyrins. Solutions of 3H(Phl^F) are emerald green in color and display broadly absorbing peaks across the UV-vis region, giving rise to the absorbance spectrum shown in Figure 2 (green trace). This absorption profile is strikingly different from the fluorinated porphyrin (2H(TpFPP)) and corrole homologues ((3H)TpFPC), as shown in Figure S3. Deviation of the phlorin electronic structure from that of typical porphyrinoids is evident from comparison of these absorption profiles. While the porphyrin exhibits narrow absorbances in the typical soret (375 – 425 nm) and Q band (490 – 530 nm and 570 – 600 nm) regions, introduction of the sp^3-hybridized center into the phlorin ring broadens these absorption bands and shifts them to longer wavelengths. Although the phlorin's absorption profile is more similar to that of the homologous corrole, which is also a trianionic ligand, the spectral coverage of the former is much greater, especially toward the low energy end of the UV-vis region. This latter observation has significant implications for light harvesting applications (*vide infra*). Figure 2 also reproduces the steady state fluorescence spectrum of 3H(Phl^F) (red trace). The emission bands of 3H(Phl^F) are the approximate mirror image of the phlorin absorption spectrum at long wavelengths with maxima at 724 and 803 nm (10

μM, THF). This emission profile is red-shifted compared to that obtained for 2H(TpFPP), which displays fluorescence bands at 640 and 702 nm in THF (10 μM).

The phlorin architecture also exhibits unique redox properties. Cyclic voltammetry expe riments carried out for 1.0 mM solutions of 3H(Phl^F) in CH_2Cl_2 containing 0.1 M $TBAPF_6$ have revealed a rich redox chemistry for this macrocycle. Figure 3 juxtaposes the CVs recorded for 3H(Phl^F) (green), 2H(TpFPP) (purple) and 3H(TpFPC) (maroon) under these conditions with an internal decamethylferrocene standard. Both 2H(TpFPP) and 3H(Phl^F) display two reduction waves at $E_{1/2}$ = –0.76 V, –1.17 V and $E_{1/2}$ = –0.98 V, –1.46 V, respectively (versus Ag/AgCl). The oxidative electrochemistry of these two porphyrinoids is more disparate, however. While 2H(TpFPP) exhibits two reversible single electron oxidative waves at relatively high potentials ($E_{1/2}$ = 1.61 V, 1.82 V), the phlorin homologue can be oxidized by up to three electrons via three discrete single electron redox events. Furthermore, all three of these oxidations occur at potentials that are more easily accessible ($E_{1/2}$ = 0.72 V, 0.99 V, 1.27 V) than even the first oxidation of the related porphyrin (2H(TpFPP)). The redox properties of 3H(Phl^F) are more similar to the homologous corrole 3H(TpFPC), which is also a trianionic porphyrinoid and displays three oxidations at $E_{1/2}$ = 0.87 V, 1.16 V, 1.39 V. These potentials are in general to slightly higher potentials than those observed for the phlorin. Similarly, the two reductions observed for 3H(Phl^F) are slightly more reversible and occur at comparable potentials compared to the corrole homologue (3H(TpFPC)), which displays redox waves at $E_{1/2}$ = –0.97 V, –1.51 V. Further analysis of these redox data show that 3H(Phl^F) has a smaller electrochemical HOMO–LUMO gap of ~1.7 eV compared to ~2.4 eV for the fluorinated porphyrin and ~1.8 eV for the fluorinated corrole. This contraction is consistent with the significant absorption bands displayed by 3H(Phl^F) at energies lower than 600 nm (*vide supra*).

Both the singly and doubly oxidized phlorin redox states are stable in solution as determined by spectroelectrochemistry experiments. Figure S4 presents the spectral changes associated with oxidation of 3H(Phl^F) by one electron and the subsequent conversion to the doubly oxidized phlorin macrocycle. Both of these conversions are reversible under the conditions of the spectroelectrochemical experiment. Oxidation of the phlorin framework is manifest in dramatic changes in the UV-vis absorption spectrum. Formation of the singly oxidized phlorin is accompanied by the formation of two intense bands to lower energies, which are centered at roughly 680 and 810 nm. Subsequent conversion to the doubly oxidized macrocycle leads to loss of these two bands and emergence of a new absorption at ~645 nm.

The phlorin also displays a notable supramolecular chemistry in addition to the unusual structural and electronic properties that distinguish this platform from more common tetrapyrrole macrocycles. Unlike typical porphyrins, the phlorin shows good selectivity for anion binding and recognition in the free base form. This behavior is well established for calixpyrroles[31,32] and other polypyrrolic platforms.[33–36] Titration of solutions of 3H(Phl^F) (10 μM) in THF with a fluoride source such as TBAF produces a series of absorbance shifts across the UV-vis region. As shown in Figure 5, fluoride binding is accompanied by increased absorptivity, especially at long wavelengths. Fluoride binding to expanded porphyrinoids[37–39] and porphyrinogens[40] is well established, and similar behavior has been reported for binding of fluoride to an expanded calix[4]pyrrole.[41] Job analysis of fluoride binding clearly demonstrates that Phl^F is capable of binding up to two F^- ions (Figure S5) to generate 3H(Phl^F)·$2F^-$. This binding stoichiometry is uncommon for simple tetrapyrrole platforms, however allosteric fluoride binding has been reported for a doubly strapped porphyrin containing two discrete anion-binding pockets.[42] In general, binding of two anions at a single polypyrrole macrocycle has only been observed for protonated porphyrinoids with higher halogens such as chloride.[43,44] By contrast, halides other than

fluoride do not readily bind to 3H(Phl^F) as judged by UV-vis spectroscopy, making the phlorin a fluoride selective halide receptor.

The ability of 3H(Phl^F) to bind two equivalents of fluoride was also confirmed by ^{19}F NMR spectroscopy. As shown in Figure S6, addition of ten equivalents of TBAF to a solution of 3H(Phl^F) in CD_3CN is accompanied by a broad resonance at –150.21 ppm, which is shifted relative to that for unbound TBAF (–115.25 ppm). The resonance corresponding to bound fluoride integrates to roughly two when normalized to the ^{19}F resonances of the fluorinated phenyl rings of the 3H(Phl^F) macrocycle.

Analysis of the titration binding data indicates that association of fluoride to the 3H(Phl^F) is highly cooperative. Well-anchored isosbestic points are maintained throughout the titration, indicating that the singly fluoride bound species is not observed. A standard Benesi-Hildebrand plot constructed from the titration data of Figure 4 is non-linear (Figure S7), indicating that the overall equilibrium is best described by the direct formation of 3H(Phl^F)·2F$^-$ from 3H(Phl^F) + 2F$^-$. In line with this, a Hill analysis[45] of the titration data produces a well-fit linear regression with a slope of ~2 confirming the 1:2 binding stoichiometry of 3H(Phl^F)·2F$^-$. The Hill plot also yields a formation constant of $\beta_2 = 1.7 \times 10^{11}$ M^{-2} for the ternary complex 3H(Phl^F)·2F$^-$, indicating that binding of the two fluoride ions is very strong. Although the individual 1:1 fluoride binding events cannot be disentangled, it is clear that the binding constant for the second fluoride ion (K_2) to generate 3H(Phl^F)·2F$^-$ is much larger than the formation constant for the first binding event (K_1), since there is no observable singly fluoride bound intermediate (3H(Phl^F)·F$^-$). While we note that previous work has demonstrated that a phlorin containing a dangling pyrrole moiety appended to the sp^3 hyrbidized *meso*-carbon can bind anions,[46] this is the first demonstration of fluoride binding to a phlorin macrocycle that does not contain an ancillary protonic residue. To the best of our knowledge, this also marks the first demonstration of how fluoride binding perturbs the UV-vis absorption of the phlorin macrocycle. It is also the first quantitative demonstration of the cooperative nature of fluoride binding to a phlorin platform.

The unusual electronic and photophysical properties of the phlorin may make this chromophore well suited for solar light harvesting. This fact is demonstrated by Figure 5, which overlays the solar power spectrum (SPS) from 300 – 900 nm onto the absorption profiles of 3H(Phl^F) and 2H(TpFPP). Although the maximal power is at ~475 nm, there is considerable contribution at longer wavelengths (λ > 550 nm) as well. While simple porphyrin derivatives display strong absorptivities in the narrow regions between ~375 – 425 and 500 – 550 nm, there are significant portions of the solar spectrum that porphyrins are unable to efficiently harvest (Figure 5a). This fact is clearly demonstrated by Figure 5a, which superimposes the absorption spectrum of 2H(TpFPP) onto the SPS. Nature confronts this issue by using carotenoids to harvest photons on the long wavelength end of the visible spectrum[47,48] and recent work has demonstrated that some cyanobacteria contain natural porphyrinoids that exhibit significant absorptivities at long wavelengths (675 – 750 nm).[49] Not surprisingly, the most efficient porphyrin based light harvesting devices rely on synthetically complex chromophores with absorption profiles that extend to ~700 nm. By contrast, the phlorin construct is much more synthetically accessible and can harvest photons across the entire UV-vis region (Figure 5a). Furthermore, the anion binding chemistry and associated spectral shifts displayed by 3H(Phl^F) presents a unique opportunity to tailor the absorption properties of this chromophore for light harvesting applications.

The ability to tune the phlorin's spectral coverage is illustrated by Figure 5b, which presents the composite UV-vis absorption profile for 3H(Phl^F) to which has been added 0.6 equivalents of TBAF (green trace). Accordingly, based on the binding stoichiometry and large association constant for fluoride binding to the phlorin macrocycle, the composition of

this solution is best described as a mixture of roughly 70% unbound 3H(Phl^F) and 30% 3H(Phl^F)·$2F^-$. This composition is confirmed by comparison to the computed absorption spectrum for this mixture, which is easily obtained by scaling and summing the spectral profiles of 3H(Phl^F) and 3H(Phl^F)·$2F^-$. This computed spectrum is overlaid onto Figure 5b (dashed orange trace). Notably, the fluoride doped 3H(Phl^F) solution closely tracks the overall shape of the SPS over most of the UV-vis region and into the near infrared. As such, the phlorin not only provides a relatively simple and synthetically accessible chromophore with enhanced absorptivities across the visible region, but also has photophysical properties that can be tuned with great facility for a given photochemical/light harvesting application. Coupled with the rich multielectron redox chemistry that the phlorin framework exhibits, this unusual chromophore possesses all the necessary characteristics to make it an excellent and inexpensive candidate for incorporation into TiO_2-based DSCs and other light harvesting devices as the sensitizer moiety.

SUMMARY AND FUTURE DIRECTIONS

The phlorin framework is an underappreciated porphyrinoid that displays a geometric and electronic structure that is distinct from more commonly studied tetrapyrrole macrocycles such as porphyrins and corroles. NMR analysis and the solid-state structure of 3H(Phl^F) clearly demonstrate that unlike typical porphyrinoids, the phlorin platform is not aromatic. As a result of this distinctive electronic structure, the phlorin displays a rich redox chemistry and can be oxidized by up to three electrons at very modest potentials. The phlorin also displays a broad UV-vis absorption profile that is significantly different from other simple porphyrinoids, especially at long wavelengths. Moreover, 3H(Phl^F) supports an intriguing supramolecular chemistry with fluoride, and can bind two equivalents of this anion. Fluoride binding to the phlorin platform is cooperative and is manifest in dramatic changes to the UV-vis profile of the chromophore, resulting in increased absorptivity and the appearance of strongly absorbing bands toward the near-IR region. The ease with which the phlorin can donate multiple electrons and the ability to tailor this compound's absorption properties via fluoride binding, makes the phlorin an intriguing candidate for incorporation into energy storing schemes and devices. It is with this goal in mind that our laboratory is pursuing the elaboration and photophysical interrogation of the phlorin family.

Supplementary Material

Refer to Web version on PubMed Central for supplementary material.

Acknowledgments

J.R. thanks Oak Ridge Associated Universities for a Ralph E. Powe Junior Faculty Enhancement Award. Additional financial support for this work was provided in part by the American Chemical Society Petroleum Research Fund, the University of Delaware Research Foundation and the University of Delaware. NMR and other data were acquired at UD using instrumentation obtained with assistance from the NSF and NIH (NSF MIR 0421224, NSF CRIF MU CHE0840401 and CHE0541775, NIH P20 RR017716).

ABBREVIATIONS

2H(TpFPP)	5,10,15,20-tetra-pentafluorophenylporphyri
3H(TpFPC)	5,10,15-tris-pentafluorophenylcorrole
SPS	solar power spectrum

REFERENCES

(1). French CS. Proc. Nat. Acad. Sci. 1971; 68:2893–2897. [PubMed: 4941990]

(2). Grätzel M. Inorg. Chem. 2005; 44:6841–6851. [PubMed: 16180840]

(3). Grätzel M. Acc. Chem. Res. 2009; 42:1788–1798. [PubMed: 19715294]

(4). Wayne M, Campbell WM, Burrell AK, Officer DL, Jolley KW. Coord. Chem. Rev. 2004; 248:1363–1379.

(5). Hagfeldt A, Boschloo G, Sun L, Kloo L, Peterson H. Chem. Rev. 2010; 110:6595–6663. [PubMed: 20831177]

(6). Campbell WM, Jolley KW, Wagner P, Wagner K, Walsh PJ, Gordon KC, Schmidt-Mende L, Nazeeruddin MK, Want Q, Grätzel M, Officer DL. J. Phys. Chem. C. 2007; 111:11760–11762.

(7). Hsieh C-P, Lu H-P, Chiu C-L, Lee C-W, Chuang S-H, Mai C-L, Yen W-N, Hsu S-J, Diau EW-G, Yeh C-Y. J. Mater. Chem. 2010; 20:1127–1134.

(8). Chang J-C, Ma C-J, Lee G-H, Peng S-M, Yeh C-Y. Dalton Trans. 2005; 8:1504–1508. [PubMed: 15824789]

(9). Wu C-H, Pan T-Y, Hong S-H, Wang C-L, Kuo H-H, Chu Y-Y, Diau EW-G, Lin C-Y. Chem. Commun. 2012; 48:4329–4331.

(10). Ripolles-Sanchis T, Guo B-C, Wu H-P, Pan T-Y, Lee H-W, Raga SR, Fabregat-Santiago F, Bisquert J, Yeh c. –Y. Diau EW-G. Chem. Commun. 2012; 48:4368–4370.

(11). Griffith MJ, Sunahara K, Wagner P, Wagner K, Wallace GG, Officer DL, Furube A, Katoh R, Mori S, Mozer A. J. Chem. Commun. 2012; 48:4145–4162.

(12). Ragoussi M-E, Cid J-J, Yum J-H, de la Torre G, Di Censo D, Gratzel M, Nazeeruddin MK, Nazeeruddin MK, Torres T. Angew. Chem. Int. Ed. 2012; 51:1–5.

(13). Bessho T, Zakeeruddin SM, Yeh C-Y, Diau EW-G, Gratzel M. Angew. Chem. Int. Ed. 2010; 49:6646–6649.

(14). Yella A, Lee H, Tsoa HN, Yi C, Chandiran AK, Nazeeruddin M, Diau EW, Yeh C, Zakeeruddin SM, Grätzel M. Science. 2011; 334:629–634. [PubMed: 22053043]

(15). Harmjanz M, Božidarević I, Scott M. J. Org. Lett. 2001; 3:2281–2284.

(16). Král V, Sessler JL, Zimmerman RS, Seidel D, Lynch V, Andrioletti B. Angew. Chem. Int. Ed. 2000; 39:1055–1058.

(17). Sessler JL, Zimmerman RS, Bucher C, Král V, Andrioletti B. Pure Appl. Chem. 2001; 73:1041–1057.

(18). Harmjanz M, Gill HS, Scott MJ. J. Am. Chem. Soc. 2000; 122:10476–10477.

(19). Bachmann J, Nocera DG. J. Am. Chem. Soc. 2004; 126:2829–2837. [PubMed: 14995200]

(20). Bachmann J, Nocera DG. J. Am. Chem. Soc. 2005; 127:4730–4743. [PubMed: 15796540]

(21). Fukuzumi S, Okamoto K, Gros CP, Guilard R. J. Am. Chem. Soc. 2004; 126:10441–10449. [PubMed: 15315460]

(22). Sheldrick GM. Acta Cryst. A. 2008; 64:112–122. [PubMed: 18156677]

(23). Callot HJ, Krattinger B. Tett. Lett. 1996; 37:7699–7702.

(24). Hong SJ, Ka JW, Won DH, Lee CH. Bull. Korean Chem. Soc. 2003; 24:661–663.

(25). O'Brien AY, McGann JP, Geier GR III. J. Org. Chem. 2007; 72:4084–4092. [PubMed: 17461598]

(26). Medforth, CJ. NMR spectroscopy of diamagnetic porphyrins. In: Kadish, KM.; Smith, KM.; Guilard, R., editors. The porphyrin handbook. Academic; San Diego: 2000. p. 1chap 35

(27). Pople JA, Untch KG. J. Am. Chem. Soc. 1966; 88:4811–4815.

(28). Aihara J, Kimura E, Krygowski TM. Bull. Chem. Soc. Jpn. 2008; 81:826–835.

(29). Gomes JANF, Mallion RB. Chem. Rev. 2001; 101:1349–1384. [PubMed: 11710225]

(30). Stepień M, Latos-Grazyński L. Top. Heterocycl. Chem. 2012:1–71.

(31). Gale PA, Sessler JL, Král V, Lynch V. J. Am. Chem. Soc. 1996; 118:5140–5141.

(32). Gale PA, Anzenbacker P Jr, Sessler JL. Coord. Chem. Rev. 2001; 222:57–102.

(33). Sessler JL, Mody TD, ford DA, Lynch V. Angew. Chem. Int. Ed. 1992; 31:452–455.

(34). Sessler JL, Cyr M, Furuta H, Král V, Mody T, Morishima T, Shinoya M, Weghorn S. Pure Appl. Chem. 1993; 65:393–398.

(35). Sessler JL, Camiolo S, Gale PA. Coord. Chem. Rev. 2003; 240:17–55.

(36). Sessler JL, Davis JM. Acc. Chem. Res. 2001; 34:989–997. [PubMed: 11747417]

(37). Shionoya M, Furuta H, Lynch V, Harriman A, Sessler JL. J. Am. Chem. Soc. 1992; 114:5714–5722.

(38). Sessler JL, Mody TD, Ford DA, Lynch V. Angew. Chem. Int. Ed. 1992; 31:452–455.

(39). Furuta H, Maeda H, Osuka A. J. Am. Chem. Soc. 2001; 23:6435–6436. [PubMed: 11427078]

(40). Gale PA, Sessler JL, Král V, Lynch V. J. Am. Chem. Soc. 1996; 118:5140–5141.

(41). Mahanta SP, Kumar BS, Baskaran S, Sivasankar C, Panda PK. Org. Lett. 2012; 14:548–551. [PubMed: 22206306]

(42). Takeuchi M, Shioya T, Swager TM. Angew. Chem. Int. Ed. 2001; 40:3372–3376.

(43). Shionoya M, Furuta H, Lynch V, Harriman A, Sessler JL. J. Am. Chem. Soc. 1992; 114:5714–5722.

(44). Zhang Y, Li MX, Lu Y, Yang H, Liu F, Li KA. J. Phys. Chem. A. 2005; 109:7442–7448. [PubMed: 16834113]

(45). Connors, KA. Binding Constants: A Measurement of Molecular Complex Stability. Wiley; New York: 1987.

(46). Ka J–W, Lee C–H. Tett. Lett. 2001; 42:4527–4529.

(47). Cogdell RJ. Phil. Trans. R. Soc. Lond. B. 1978; 284:569–579.

(48). Siefermann-Harms D. Physiol. Plantarum. 1987; 69:561–568.

(49). Chen M, Schliep M, Willows RD, Cai Z-L, Neilan BA, Scheer H. Science. 2010; 329:1318–1319. [PubMed: 20724585]

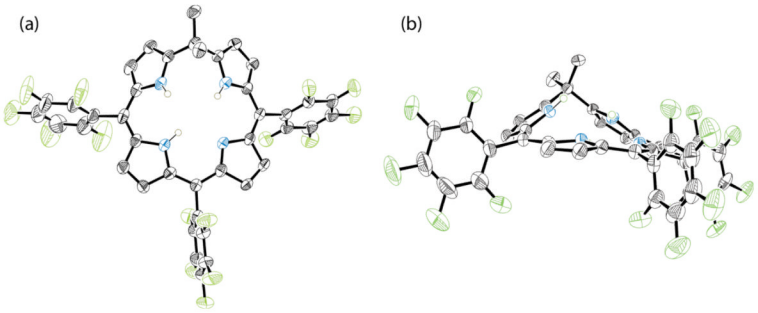

Figure 1.

Solid-state structure of 3H(Phl^F) shown from (a) above the plane of the macrocycle and (b) side on. The reduced side of the phlorin is displaced 0.60 Å above the rest of the macrocycle. A molecule of cocrystallized $CHCl_3$ and all non-nitrogen bound hydrogen atoms have been omitted for clarity.

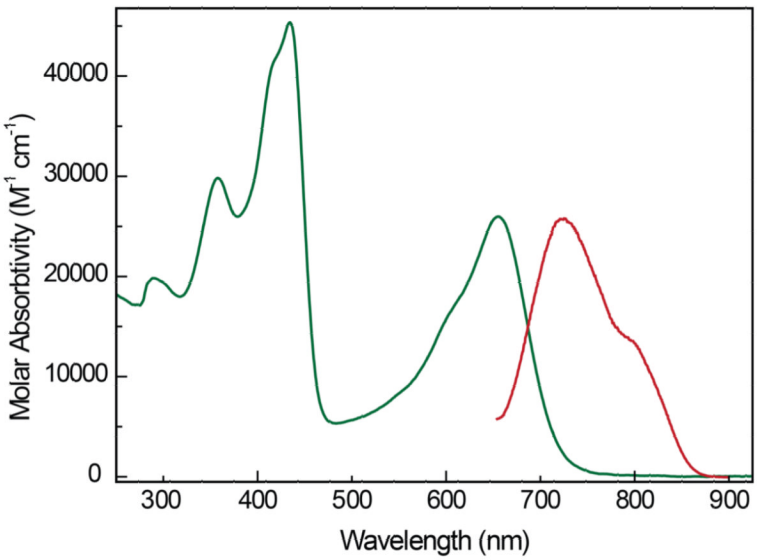

Figure 2.
UV-vis absorption (green) and normalized emission (red) spectra recorded for a 10 μM solution of Phl^F in THF.

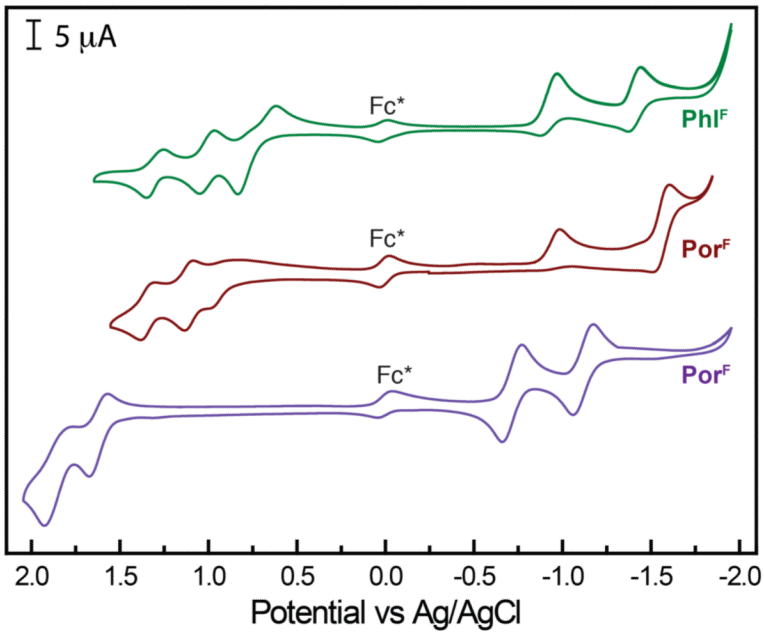

Figure 3.

Cyclic voltammograms recorded using a scan rate of 50 mV/s for 3H(Phl^F) (green), 3H(TpFPC) (maroon) and 2H(TpFPP) (purple) in CH_2Cl_2 containing 0.1 M $TBAPF_6$ with an internal decamethylferrocene standard (Fc*).

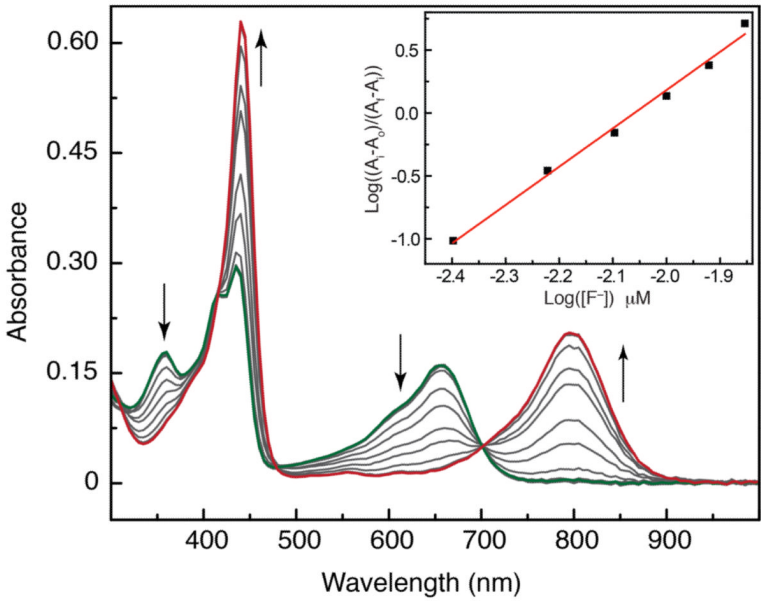

Figure 4.

Changes in the UV-vis absorption spectrum of Phl^F upon titration with TBAF. Inset: Hill plot constructed for fluoride binding to generate $3H(Phl^F) \cdot 2F^-$.

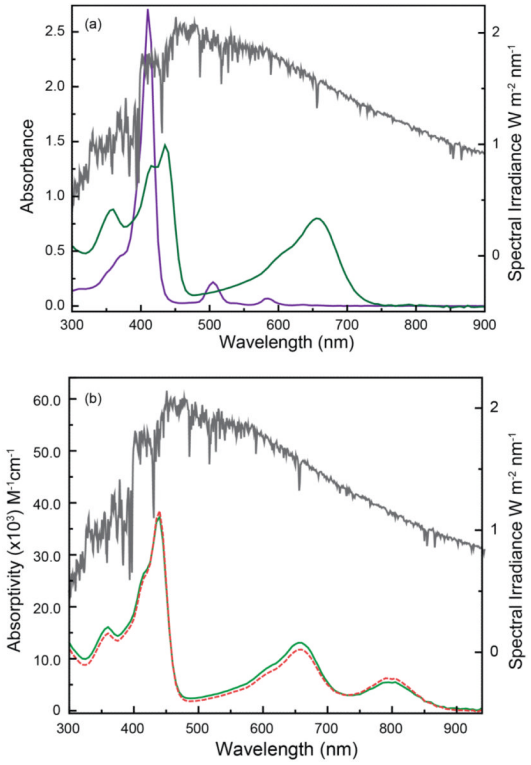

Figure 5.

(a) Comparison of the UV-vis absorption profiles of 2H(TFPP) and 3H(Phl^F) μ superimposed onto the SPS; (b) Superposition of the SPS onto the absorption profile of 10 M 3H(Phl^F) + 0.6 equiv. of TBAF in THF (green) and the calculated spectrum obtained for a · solution of 70% 3H(Phl^F) and 30% 3H(Phl^F) $2F^-$ (dashed orange).

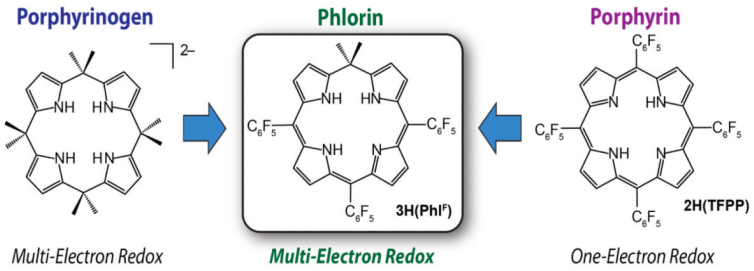

Scheme 1.
Strategy adapted for development of the phlorin architecture.

Table 1

Crystal Data and Structure Refinement for $3H(Phl^F)\cdot CHCl_3$.

Empirical formula	$C_{41}H_{18}Cl_3F_{15}N_4$	
Formula weight	957.94	
Temperature	100(2) K	
Crystal system	Monoclinic	
Space group	$P2_1$	
Unit cell dimensions	a = 15.2855(5) Å	
	b = 9.2994(3) Å	β= 116.573(2)°
	c = 15.5097(5) Å	
Volume	1971.75(11) $Å^3$	
Z	2	
Density (calculated)	1.613 mg/m^3	
Absorption coefficient	3.102 mm^{-1}	
F(000)	956	
Crystal size	0.44 × 0.04 × 0.04 mm^3	
Q range for data collection	3.19 to 70.53°	
Index ranges	$-18 \le h \le 18$, $-9 \le k \le 10$, $-18 \le l \le 18$	
Reflections collected	31054	
Independent reflections	6920 [R_{int} = 0.0476]	
Completeness to Q = 68.00°	98.4 %	
Absorption correction	Numerical	
Max. and min. transmission	0.8965 and 0.3423	
Refinement method	Full-matrix least-squares on F^2	
Data / restraints / parameters	6920 / 46 / 601	
Goodness-of-fit on F^2	1.030	
Final R indices [I>2σ(I)]	R_1 = 0.0556, wR_2 = 0.1526	
R indices (all data)	R_1 = 0.0624, wR_2 = 0.1587	
Absolute structure parameter	0.06(2)	
Largest diff. peak and hole	0.662 and −0.341 e/$Å^{-3}$	